Article

Immobilization of Horseradish Peroxidase for Phenol Degradation

Can Liu, Li Tan, Kaixin Zhang, Wenyi Wang, and Lanqing Ma*

Cite This: *ACS Omega* 2023, 8, 26906−26915

Read Online

ACCESS | Metrics & More | Article Recommendations | SI Supporting Information

ABSTRACT: The use of enzymes to degrade environmental pollutants has received wide attention as an emerging green approach. Horseradish peroxidase (HRP) can efficiently catalyze the degradation of phenol in the environment; however, free HRP exhibits poor stability and temperature sensitivity and is easily deactivated, which limit its practical applications. In this study, to improve their thermal stability, HRP enzymes were immobilized on mesoporous molecular sieves (Al-MCM-41). Specifically, Al-MCM-41(W) and Al-MCM-41(H) were prepared by modifying the mesoporous molecular sieve Al-MCM-41 with gluta-raldehyde and epichlorohydrin, respectively, and used as carriers to immobilize HRP on their surface, by covalent linkage, to form the immobilized enzymes HRP@Al-MCM-41(W) and HRP@Al-MCM-41(H). Notably, the maximum reaction rate of HRP@Al-MCM-41(H) was increased from 2.886×10^5 (free enzyme) to 5.896×10^5 U/min^{-1}, and its half-life at 50 °C was increased from 745.17 to 1968.02 min; the thermal stability of the immobilized enzyme was also significantly improved. In addition, we elucidated the mechanism of phenol degradation by HRP, which provides a basis for the application of this enzyme to phenol degradation.
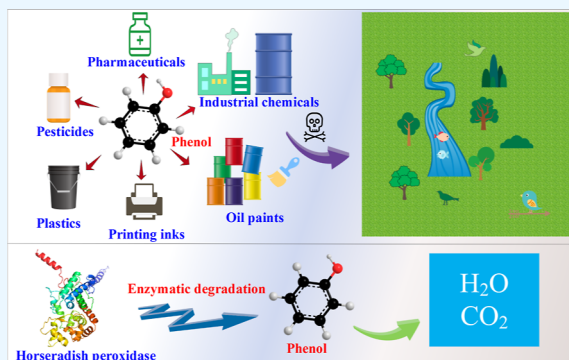
1. INTRODUCTION

Phenol is a widespread toxic environmental pollutant that is threatening the survival of organisms and the health and safety of human life.[1] Phenol is a raw material for the synthesis of many chemical products and intermediates and is therefore of significant industrial importance (Figure 1). In particular, this
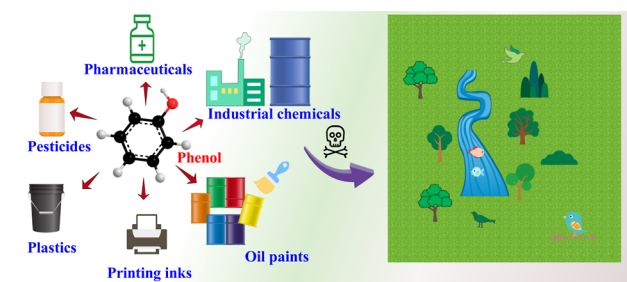

Figure 1. Widespread use of phenol and potential environmental damage from phenol leakage.

compound is used as a solvent, experimental reagent, and disinfectant in the pharmaceutical industry. Moreover, it is an important raw material for pesticide production and is widely used in agriculture. Notably, the pharmaceutical, printing, and dyeing industries produce large amounts of phenol-containing wastewater,[2] which are difficult to eliminate from the environment over a short period. Owing to the large-scale use of phenol and its derivatives, leakage into the environment can cause serious environmental pollution.[3] Therefore, artificial

assistance is needed to accelerate the degradation of phenol in the environment. The current degradation pathways of phenol include adsorption, electrochemical[4] and Fenton oxidation, photodegradation,[5] ultrasonic degradation,[6] and ozone oxidation; microbial and enzymatic degradation pathways are also available.

In the adsorption method, phenol in the environment is removed by intermolecular van der Waals forces using adsorbents such as activated carbon and bentonite.[7,8] However, this method does not degrade phenol and is susceptible to external environmental factors. Moreover, phenol is resolved from the carrier, thereby triggering secondary pollution.[9]

Electrochemical methods mainly use oxygen radicals generated by ionization or other strong oxidizing substances to oxidatively degrade phenol in the environment.[10] This method is safer, simpler, and more convenient than the other chemical oxidative degradation methods.[4] However, during the electrochemical degradation of phenol, the quinones produced from the reaction form polymers that attach to the surface of the metal oxide electrode and deactivate it.[11] Although these

electrodes can be reused, electrode reconstruction is expensive; thus, this method is not widely used in practical applications.

Fenton oxidation is a process in which Fe^{2+} catalyzes the generation of hydroxyl radicals from H_2O_2 under acidic conditions to oxidatively degrade pollutants to CO_2 and H_2O.[12,13] The H_2O_2 in the system promotes the mutual transformation of Fe^{2+} and Fe^{3+} to co-catalyze the reaction and realize the chain cycle of the reaction system to rapidly degrade the phenol present in wastewater;[14] however, the traditional Fenton method displays low efficiency and high cost for H_2O_2 utilization.

The biodegradation of pollutants is an effective and environmentally friendly method of environmental remediation. The main biodegradation pathways are microbial degradation and enzymatic degradation. The microbial strains commonly used for phenol degradation are *Staphylococcus*,[15] *Bacillus*,[16] *Pseudomonas*,[17] and *Rhodococcus erythropolis*;[18] however, phenol is cytotoxic and inhibits the growth and reproduction of microorganisms. Moreover, toxic substances such as heavy metal ions, phenolic derivatives, and azo dyes may be present in high concentrations in phenolic wastewater, which also inhibit bacterial growth and nitrification,[19] thereby decreasing the efficiency of the bacterial degradation pathway. The enzymatic degradation of environmental pollutants has received wide attention in recent years as an emerging green approach, with the main enzymes used for phenol degradation being laccase,[20] peroxidase,[21] tyrosinase,[22] and phenol hydroxylase.[23] The enzymatic reaction conditions are mild and benevolent to the environment; however, the spatial conformation of enzyme molecules is easily affected by high temperature and pH in the environment, and enzymes are prone to deactivation, thereby limiting their application in phenol degradation.[24]

Horseradish peroxidase (HRP) is widely employed in environmental treatment and is commonly used to degrade benzene and aniline;[25] however, owing to its instability and non-recyclability, the production cost is high, thereby limiting its applicability. Therefore, improving the stability of HRP is an urgent problem to be solved. Enzyme immobilization is an enzyme engineering technology that can improve the stability of enzymes with broad application prospects in environmental remediation.[26]

Molecular sieves are excellent carriers for enzyme immobilization because of their good chemical stability and large specific surface area.[27] Al-MCM-41 is a molecular sieve with a hexagonally ordered mesoporous structure. It has a high specific surface area and high adsorption capacity. Notably, the surface of Al-MCM-41 contains hydroxyl groups, which facilitates binding with enzymes.[28,29] Al-MCM-41 has received much attention from domestic and foreign scholars as an excellent catalyst carrier for chemical, pharmaceutical, environmental protection, adsorption, and separation applications. To the best of our knowledge, the immobilization of HRP using the molecular sieve Al-MCM-41 has not been reported to date. Thus, in this study, we immobilized HRP onto the surface of glutaraldehyde/epichlorohydrin graft-modified Al-MCM-41 mesoporous molecular sieve carriers by covalent linkages for the degradation of phenol and studied the resultant phenol degradation mechanism.

2. MATERIALS AND METHODS

2.1. Preparation of the Immobilized Enzymes.
A glutaraldehyde-grafted Al-MCM-41(W) carrier was prepared as follows (Figure S1A). First, 27.5 mL of distilled water was added to 5 g of Al-MCM-41 (Nankai University Catalyst, China), followed by 3 mL of glutaraldehyde and 0.5 mL of 12 M HCl. The mixture was shaken for 3 h at 40 °C to ensure that the carrier and glutaraldehyde were mixed well. Subsequently, the mixture was centrifuged at 2500 r·min⁻¹ for 10 min, and the supernatant was discarded. The precipitate was washed with phosphate buffer (pH 7) to neutral and freeze-dried (Alpha 2-4 LSCplus, Marin Christ, Germany) to obtain Al-MCM-41(W).

Next, an epichlorohydrin-grafted Al-MCM-41(H) carrier was prepared as follows (Figure S1B). First, 23 mL of distilled water was added to 5 g of Al-MCM-41, followed by 5 mL of epichlorohydrin and 2 mL of 2 M NaOH. The mixture was shaken for 8 h at 40 °C to ensure that the carrier and epichlorohydrin were mixed well. Subsequently, the mixture was centrifuged at 2500 r·min⁻¹ for 10 min, and the supernatant was discarded. The precipitate was washed with phosphate buffer (pH 7) to neutral and freeze-dried (Alpha 2-4 LSCplus) to obtain Al-MCM-41(H).

To obtain the immobilized enzymes, HRP (A600691, Sangon Biotech, China) was dissolved in phosphate buffer (pH 7) to obtain a concentration of 1 mg·mL⁻¹. Next, the grafted carrier [Al-MCM-41(W) or Al-MCM-41(H)] was mixed with the enzyme solution at a carrier (g)-to-enzyme solution (mL) ratio of 1:600 and shaken at 25 °C for 8 h. The mixture was then centrifuged at 2500 r·min⁻¹ for 10 min, and the supernatant was discarded. The precipitate was washed with phosphate buffer (pH 7) to obtain the immobilized enzymes HRP@Al-MCM-41(W) and HRP@Al-MCM-41(H), respectively.

The morphologies of the carriers and grafted carriers were studied using field emission scanning electron microscopy (FE-SEM; JEOL, JSM-6700F, Japan). The pore size of the samples was determined using a specific surface area analyzer (AUTOSOBIQ2-MP, Quantachrome Co., USA), and the average pore-size distribution was calculated using the Barrett−Joyner−Halenda method. The chemical group composition of the sample surface was analyzed using infrared spectroscopy (Cary 630, Agilent Technologies Inc., USA) in the reflection spectroscopy mode, and the sample was placed on the detection platform. The scan range, scan number, and resolution were 450−4000, 32, and 2 cm⁻¹, respectively. X-ray powder diffraction (XRD; D8, Bruker, Germany) was conducted at 35 kV at a scan speed of 1°·min⁻¹.

2.2. HRP Activity Assay.
HRP activity tests were conducted according to the standard GB/T32131-2015. To determine the enzyme activity, 0.8 mL of 0.1 mol·L⁻¹ phosphate-buffered saline (PBS; pH 7) was placed in a centrifuge tube along with 0.1 mL of 20 mmol·L⁻¹ guaiacol solution, 0.05 mL of 8 mmol·L⁻¹ hydrogen peroxide solution, and finally 0.05 mL of enzyme suspension. The reaction was rapidly performed for 2 min, followed by centrifugation at 6000 r·min⁻¹ for 1 min. The absorbance of the supernatant was then measured at 436 nm using a spectrophotometer (Unico2100, UNICO Instrument Co., Ltd., China). The amount of enzyme that converted 1 mmol of H_2O_2 per minute with an average of 1 mg of protein was defined as one enzyme activity unit (1 U).

2.3. Effect of Temperature and pH on the Enzyme Activity.
To study the effect of pH on the enzyme activity, the HRP activity was assayed at 25 °C using different pH buffer systems: acetic acid−sodium acetate buffer (pH 4−5),

phosphate buffer (pH 6–8), and glycine–sodium hydroxide buffer (pH 9–10). To study the effect of temperature on the enzyme activity, the enzyme + substrate mixture was placed in a water bath at different temperatures (25, 30, 35, 40, 45, 50, 55, and 60 °C) for 30 min and mixed well. The enzyme activity at different temperatures was then measured according to Section 2.2. The highest enzyme activity measured was defined as 100% for both the free and immobilized enzymes.

2.4. Determination of the Enzyme Kinetic Constants. We proceeded to test the effect of different substrate concentrations on the rate of the enzymatic reaction to establish an enzyme kinetic equation. Thus, guaiacol solutions of different concentrations (1, 2, 5, 6, 8, 10, 15, 20, 50, and 100 mM) were first prepared using distilled water. The immobilized enzyme suspension (0.05 g·mL^{-1}) and 8 mM H$_2$O$_2$ were maintained at 45 °C for 30 min. Immediately after, 0.8 mL of buffer solution, 100 μL of guaiacol solution, 50 μL of H$_2$O$_2$ solution, and 50 μL of enzyme solution were mixed, and the reaction was allowed to proceed for 2 min. The mixture was then immediately centrifuged at 6000 r·min^{-1} for 1 min, and the change in optical density at 436 nm (OD$_{436}$) was measured within 2 min using an UV–visible spectrophotometer. The kinetic constants of the enzyme activity were calculated from the Lineweaver–Burk plots using the equation[30]

$$\frac{1}{V} = \frac{K_{\mathrm{m}}}{V_{\mathrm{max}}} \cdot \frac{1}{[S]} + \frac{1}{V_{\mathrm{max}}} \tag{1}$$

where V is the reaction velocity, S is the concentration of the guaiacol substrate (mM), K_{m} is the Michaelis–Menten constant, and V_{max} is the maximum reaction velocity.

2.5. Determination of the Thermal Stability of HRP. High temperature can promote molecular movement; however, too high a temperature can change the spatial conformation of enzyme molecules, leading to enzyme inactivation. Thus, the enzymes were maintained at 50–60 °C for 0–160 min, and the enzyme activity was measured at different time points. The decay rate constant k_{d} for enzyme inactivation at different temperatures was then calculated.

According to enzyme inactivity mechanics

$$-\frac{\mathrm{d}V_t}{\mathrm{d}t} = k_{\mathrm{d}} \cdot V_t \tag{2}$$

where V_t is the enzyme reaction rate at time t. Solving the two-sided integral in eq 2 gives

$$V_t = V_0 \exp(-k_{\mathrm{d}} \cdot t) \tag{3}$$

where V_0 is the enzyme reaction rate at time t_0 and t is the reaction time. Taking the natural logarithm on both sides simultaneously in eq 3 gives

$$\ln V_t = -k_{\mathrm{d}} \cdot t + \ln V_0 \tag{4}$$

The conformational change of a protein due to heat and consequent loss of activity is termed thermal inactivation, and the activation energy required for enzyme thermal deactivation is referred to as E_{d}. The value of E_{d} can be calculated using the Arrhenius formula[31,32]

$$\ln \frac{k_{\mathrm{d2}}}{k_{\mathrm{d1}}} = -\frac{E_{\mathrm{d}}}{R}\left(\frac{1}{T_2} - \frac{1}{T_1}\right) \tag{5}$$

where R is the gas constant (8.314 J·mol^{-1}·K^{-1}), and k_{d1} and k_{d2} are the decay rate constants of the enzyme at temperatures T_1 and T_2, respectively.

The rate of enzyme inactivation is usually expressed in terms of the half-life ($t_{1/2}$; eq 6) and D-value (eq 7), which are defined as the time taken for the enzyme activity to be reduced by 50 and 90%, respectively, at a given temperature.

$$t_{1/2} = \frac{\ln 2}{k_{\mathrm{d}}} \tag{6}$$

$$D = \frac{\ln 10}{k_{\mathrm{d}}} \tag{7}$$

2.6. Storage Stability and Reusability of the Immobilized Enzymes. Storage stability is an important parameter to evaluate the performance of biological enzymes. Enzymes are exposed to the environment for a long time, and the enzyme activity gradually decreases with prolonged storage time because of the influence of temperature and light. The free and immobilized enzymes were stored for 30 d at a temperature of 4 or 25 °C in a dark environment, and the residual activity of the enzymes was measured every 5 d. The activity of the enzyme measured on the first day was taken as 100%, after which the enzyme activity was calculated for the different storage times to study the storage stability of the enzyme. The reusability of the HRP@Al-MCM-41(W) and HRP@Al-MCM-41(H) catalysts was measured by employing the catalysts in HRP activity assays (Section 2.2). The immobilized enzymes were then separated from the substrate solution by centrifugation and washing three times with 3.5 mL of 0.1 mol·L^{-1} PBS (pH 7), after which the HRP activity assays were repeated under the same conditions. Six enzymatic degradation–separation cycles were conducted.

2.7. Application of the Enzymes to Phenol Degradation. To investigate the applicability of the enzymes to phenol degradation, 2.5 mL of phosphate buffer (20 mM, pH 7) was placed in a centrifugal tube, followed by adding hydrogen peroxide (200 μL, 8 mM) and the immobilized enzyme suspension (50 μL, mg·g^{-1}), and then phenol solution (300 μL, 10 mM). The resultant mixture was mixed well and incubated at 45 °C, and samples were collected after 10, 20, 30, 40, and 50 min. The collected samples were immediately centrifuged at 6000 r·min^{-1} for 10 min, filtered through a 0.22 μm membrane (Tianjin Keyilong Lab Equipment Co., Ltd., China), and finally analyzed using high-performance liquid chromatography (HPLC; Agilent 6470, Agilent Technologies Inc., USA) to determine the phenol concentrations at the different collection times. The HPLC conditions were as follows: separation column, Agilent SB-C18, 4.6 × 150 mm, 5 μm, with a PDA detector; detection wavelength, 270 nm; and column temperature, 30 °C. The mobile phases were deionized water (phase A) and acetonitrile (phase B). Elution was performed using a 3:7 acetonitrile-to-water ratio at a mobile phase flow rate of 0.8 mL·min^{-1}, and a sample volume of 10 μL was injected for analysis.

The mass spectrometry detection conditions were as follows: separation column, Agilent SB-C18 4.6 × 150 mm, 5 μm. The mobile phases were acetonitrile (mobile phase A) and water (mobile phase B) eluted according to a 3:7 program with a split ratio of 1:3 and an injection volume of 2 μL. The m/z scan range of mass spectrometry detection was in the range of 50–250, with a scan speed of 17,000 Da·s^{-1} and scan
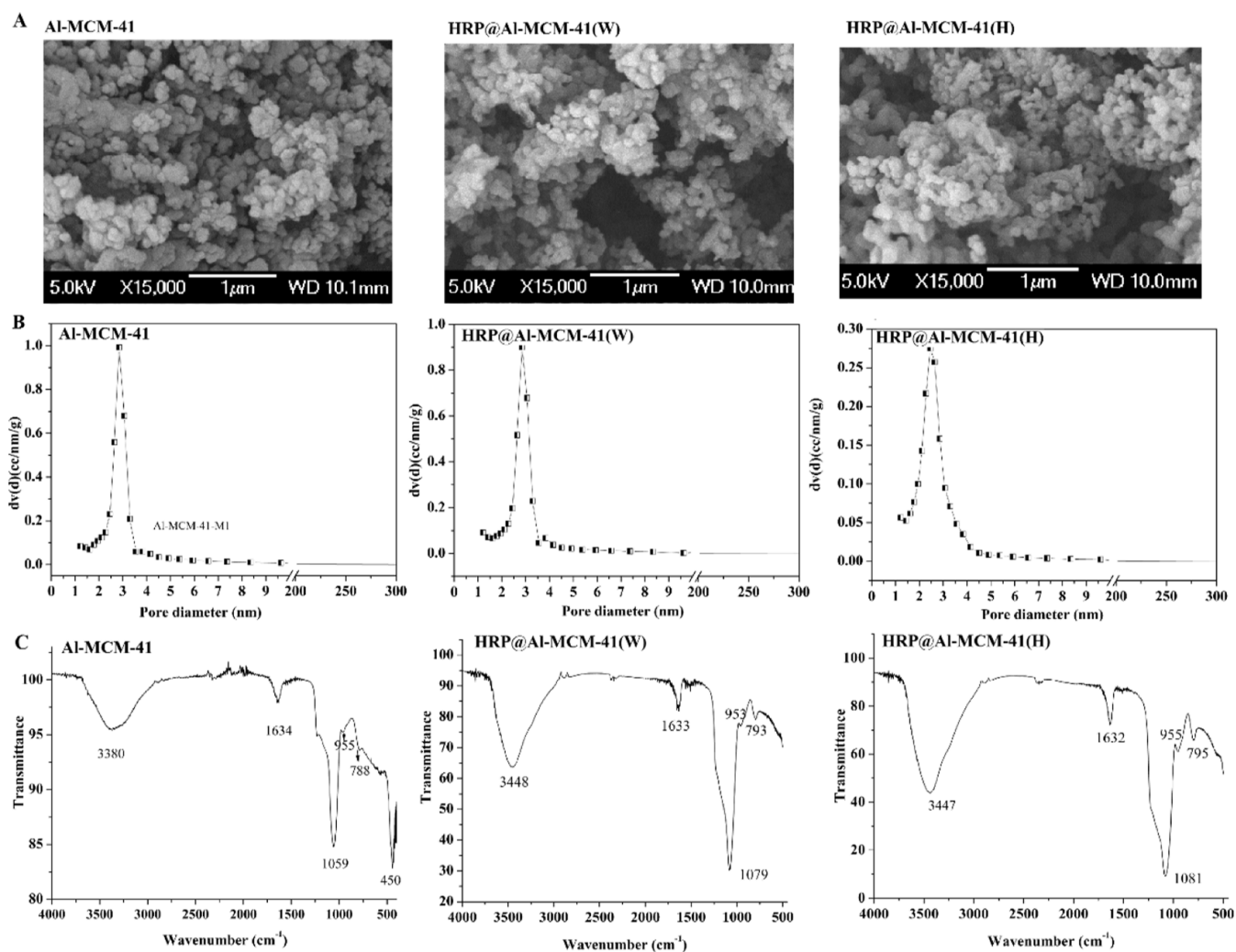
Figure 2. Characterization of the Al-MCM-41 carrier and immobilized HRP catalysts. (A) SEM images, (B) pore-size distributions, and (C) FT-IR spectra of Al-MCM-41, HRP@Al-MCM-41(W), and HRP@Al-MCM-41(H).

time of 15 min in the anion detection mode. Nitrogen was used as the protective gas, and the AJS ESI ion source was used for detection with a spray voltage of 3500 V, atomization pressure of 45 psi, and capillary temperature of 250 °C.

2.8. Statistical Analysis. The data in this work are the mean ± standard deviation (SD) of three replicate independent experiments.

3. RESULTS AND DISCUSSION

3.1. Characterization of the Immobilized Horseradish Enzymes. As shown in Figure 2A, the morphology of the Al-MCM-41 carrier does not significantly change after the enzyme is immobilized, indicating that grafting of the carrier and the enzyme immobilization process does not damage its structure. Moreover, Figure 2B reveals that Al-MCM-41 is a mesoporous material with a pore-size distribution mainly in the range of 2–4 nm. The pore sizes of the immobilized enzymes, HRP@Al-MCM-41(W) and HRP@Al-MCM-41(H), are also in this range. This indicates that enzyme immobilization does not block the pores of the carrier, and therefore, the pore size of the immobilized enzyme does not decrease.

Figure 2C shows the IR spectra of the carrier Al-MCM-41 and immobilized enzymes HRP@Al-MCM-41(W) and HRP@Al-MCM-41(H). In the IR spectrum of Al-MCM-41, the signal at 3380 cm^{-1} is assigned to the H_2O or Si−OH vibrational absorption peak, that at 1634 cm^{-1} to the H−O−Al or water OH vibrational absorption peak, those at 1059 and 788 cm^{-1} to T−O−T (T is Al or Si) antisymmetric or symmetric stretching vibrational absorption peaks, that at 955 cm^{-1} to the Si−OH symmetric stretching vibrational peak, and that at 450 cm^{-1} to the Al-MCM-41 molecular backbone Si−O−Si bending stretching peak.

For the immobilized HRP@Al-MCM-41(W), the −OH vibrational absorption peak at 3448 cm^{-1} is enhanced, indicating that a large amount of C−OH is introduced after the enzyme is immobilized on the carrier. Moreover, a smaller absorption peak appeared at 1633 cm^{-1}, probably because of the amide spectrum generated by the enzyme on the carrier surface. This absorption peak is weak, owing to the small amount of enzyme immobilization. A sharper absorption peak appeared at 1079 cm^{-1}, where the absorption peak markedly shifted to a lower wavenumber relative to that of the empty carrier. This is ascribed to the −C≡N bond introduced by enzyme linkage to the carrier and the amide bond of the enzyme, indicating a shift in the T−O−T absorption peak. Finally, a small absorption peak at 793 cm^{-1} is assigned to N−H bending vibrations. Near-identical results are observed in the HRP@Al-MCM-41(H) spectrum. We characterized the
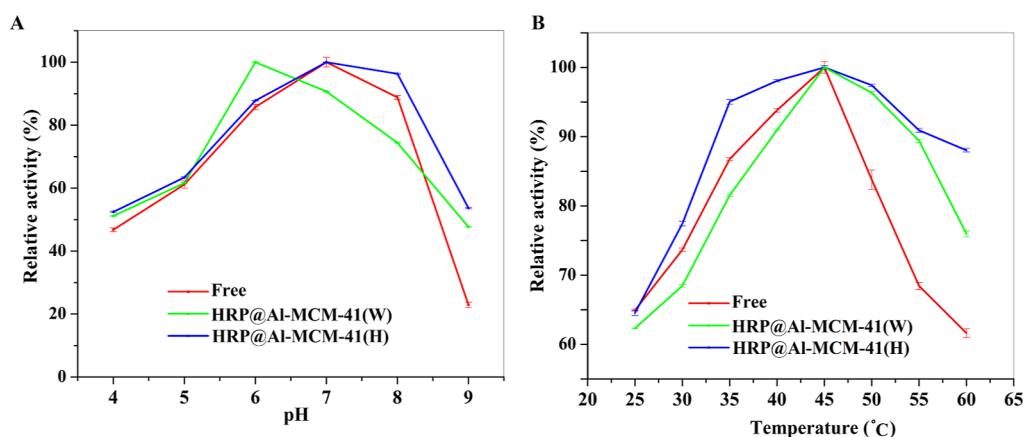
Figure 3. Effect of pH and temperature on the activity of the free and immobilized HRP. Effect of (A) pH and (B) temperature on the activity of the free HRP, HRP@Al-MCM-41(W), and HRP@Al-MCM-41(H) enzymes.
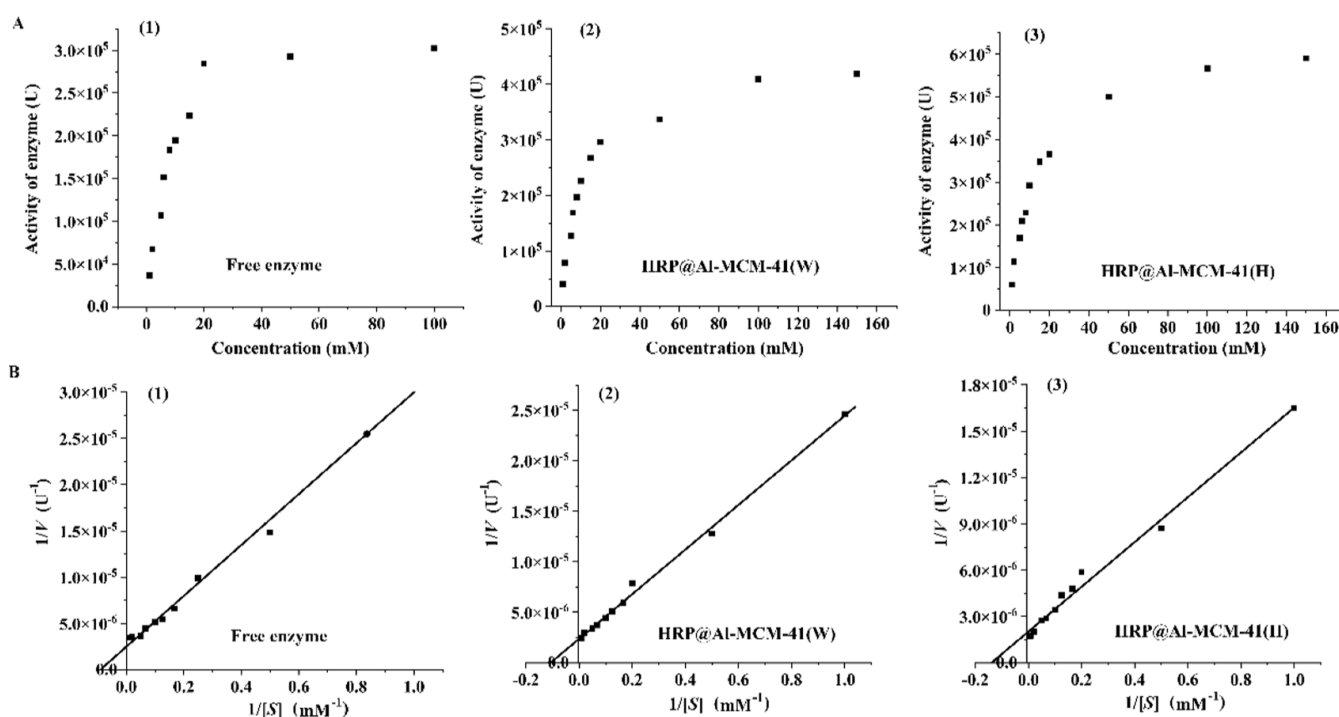

Figure 4. Substrate saturation curves and Lineweaver−Burk plots of HRP. (A) Substrate saturation curves for the peroxidase-catalyzed reactions and (B) Lineweaver−Burk plots of HRP for the (1) free enzyme, (2) HRP@Al-MCM-41(W), and (3) HRP@Al-MCM-41(H).

structure of the carrier Al-MCM-41 and the immobilized enzymes by XRD (Figure S3). The results show that the Al-MCM-41 carrier still has a regular hexagonal mesoporous structure after the immobilization of HRP, and the crystalline structure of the carrier is not damaged.

3.2. Effect of pH and Temperature of the Reaction Medium on the Enzymatic Reactions. As shown in Figure 3A, the enzyme activity is regulated by pH. The optimum pH of the free enzyme is determined to be pH 7, while those of the immobilized enzymes HRP@Al-MCM-41(W) and HRP@Al-MCM-41(H) are pH 6 and 7, respectively. When the pH of the reaction system is >8, the enzyme activity begins to rapidly decrease, and at pH 9, the residual activity of the free enzyme is 20%, while those of the immobilized enzymes are ≥40%. Thus, compared with the free enzyme, the immobilized enzymes are less likely to be affected by the pH. The immobilized enzyme HRP@Al-MCM-41(W) has a lower

optimal pH than the free enzyme because the aldehyde group on Al-MCM-41(W), introduced during glutaraldehyde grafting, reacts with the free amino group of the protein during the aldehyde−amine condensation reaction, while simultaneously immobilizing the protein on the carrier. This changes the microenvironment around the immobilized enzyme and consequently changes its optimum pH. Similar changes in the optimal pH for the enzyme activity of HRP after immobilization have also been reported previously.[33,34] For example, Katarzyna et al.[35] reported that the optimal pH for HRP activity was lower (more acidic) after immobilization on electrospun fibers.

Figure 3B reveals that the free enzyme activity gradually increases between 25 and 45 °C but decreases at 50 °C, in agreement with the results of Lopes et al.[36] Moreover, the residual activity at 60 °C approximates 60% for the free enzyme, 75% for the immobilized enzyme HRP@Al-MCM-
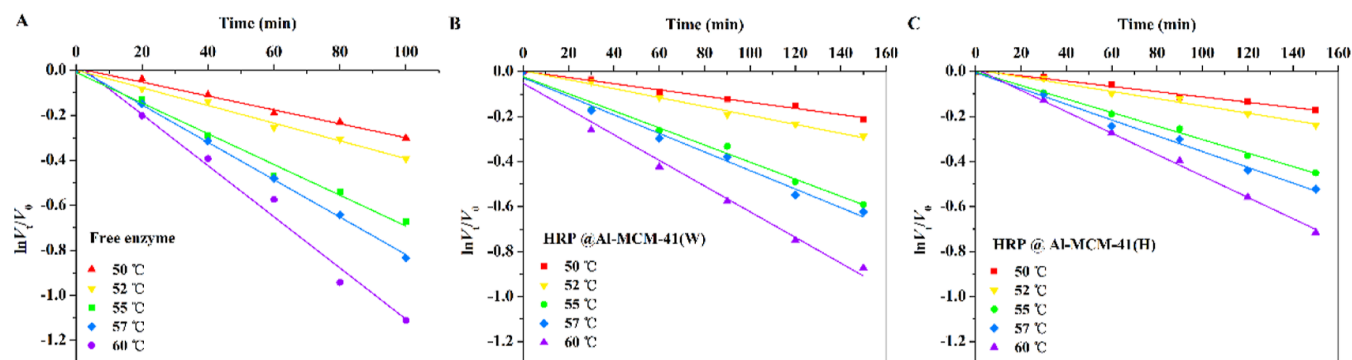
Figure 5. First-order thermal deactivation plots of free and immobilized HRP at different temperatures: (A) free enzyme, (B) HRP@Al-MCM-41(W), and (C) HRP@Al-MCM-41(H).
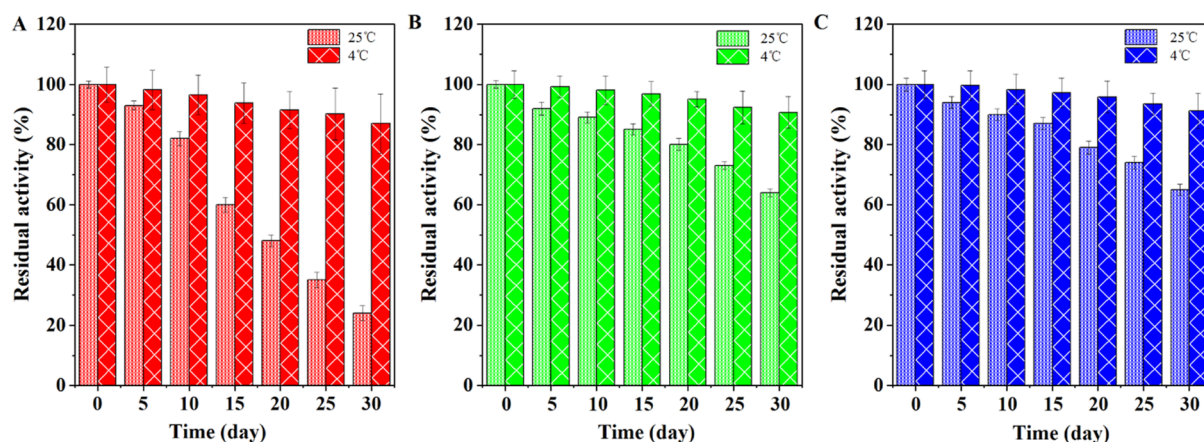

Figure 6. Effect of storage temperature on the activity of free and immobilized HRP. (A) Free enzyme, (B) HRP@Al-MCM-41(W), and (C) HRP@Al-MCM-41(H) stored at 4 and 25 °C.

41(W), and 87% for the immobilized enzyme HRP@Al-MCM-41(H). The decrease in free enzyme activity with increasing temperature occurs because the increase in temperature tends to loosen the conformation, mobility, and vibration of the enzyme,[37] thereby destroying the tertiary structure of the enzyme protein. However, after HRP is immobilized, the stability of the enzyme structure is enhanced; hence, more energy is required to destroy the enzyme structure. Thus, the immobilized enzymes are more stable than the free enzyme.

3.3. Enzyme Kinetic Analysis. Figure 4 reveals that the activities of all three enzyme samples gradually increase with the gradual increase in the substrate concentration. Moreover, the enzyme activity tends to stabilize when the substrate reaches a certain concentration, indicating that the enzyme reaches the maximum reaction velocity (V_{max}). Plotting the enzymatic reaction velocity against the substrate concentration produces a hyperbolic curve, indicating that HRP displays Michaelis−Menten enzyme kinetics. The Michaelis−Menten constant (K_m) and V_{max} were calculated from the Lineweaver−Burk plots and are listed in Table S1. After immobilization, the K_m values of the immobilized enzymes increase compared with that of the free enzyme, indicating that the affinities of the immobilized enzymes to the substrates are lower than that of the free enzyme.[38] This is attributed to the binding of the enzyme to the carrier, which increases the spatial site resistance of the enzyme to the substrate and restricts the movement of the enzyme in the reaction system, thereby reducing the ability of the enzyme to bind to the substrate.[39] As a result, the

activities of the immobilized enzymes are higher than that of the free enzyme. In particular, the activity of HRP@Al-MCM-41(H) is 104% higher than that of the free enzyme. This may be because immobilization changes the structure of the enzyme and activates its catalytic activity center, thereby accelerating the velocity and catalyzing the conversion of the substrate. HRP catalysis occurs by a ping-pong reaction mechanism, in which the enzymes form transition intermediates with the substrate. However, generated superoxide anions can combine with these enzyme−substrate intermediates to form complexes, which reduces the activity of the active enzyme and inhibits the production of the product. Al-MCM-41 carriers, which have several Brønsted and Lewis acid sites, can reduce the superoxide anions and therefore decrease the production of complexes,[40] thus improving the enzyme activity.

3.4. Thermal Inactivation of the Enzymes. We next analyzed the thermal stability of the enzyme. As shown in Figure 5, at reaction temperatures of 50−60 °C, the residual enzyme activity gradually decreases with increasing temperature for the same heat treatment time. The slope of the deactivation plot represents the enzyme deactivation rate constant k_d, which is positively correlated with the enzyme heat treatment temperature.[41] Thus, as the heat treatment temperature increases, the slope (k_d) also increases, wherein a high k_d value indicates that the enzyme is unstable and prone to thermal deactivation.

The free enzyme presents the highest k_d value, indicating that the free enzyme is the most likely to be inactivated at high temperatures, whereas the immobilized enzyme HRP@Al-
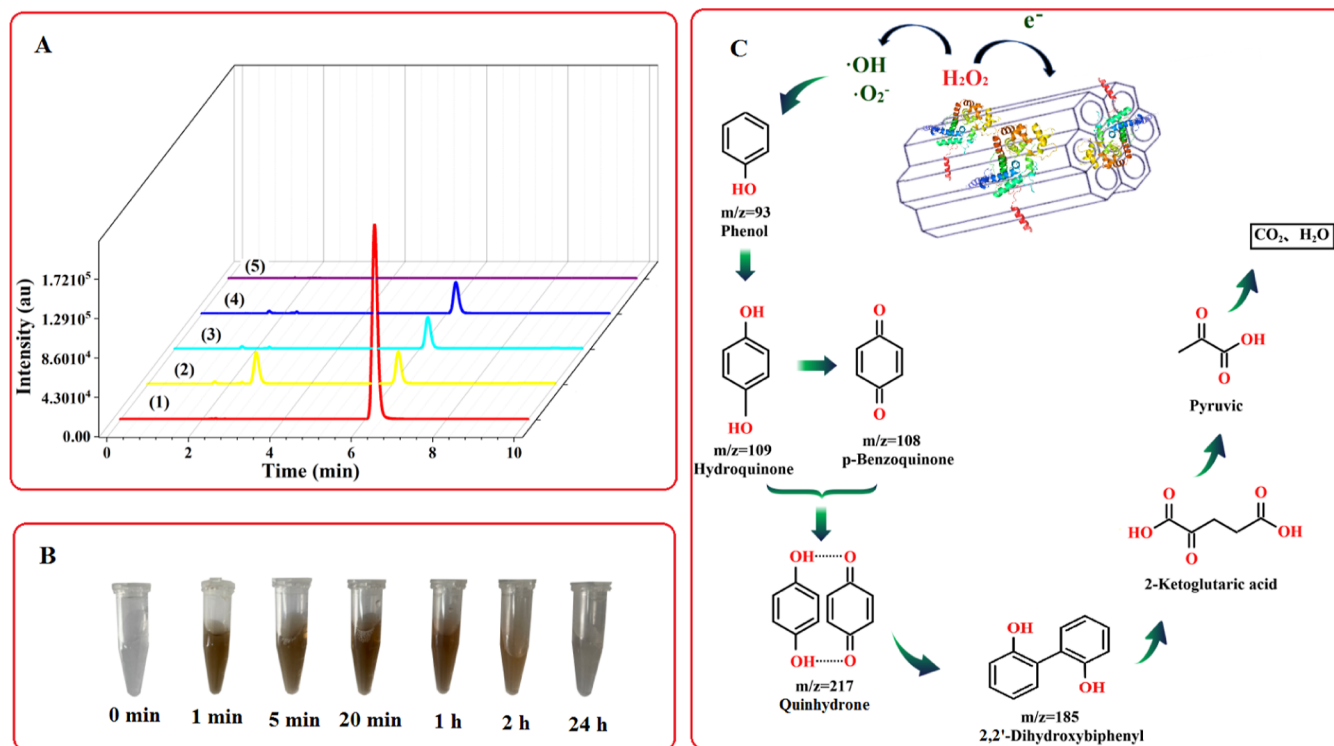
Figure 7. Enzymatic degradation of phenol and phenol degradation pathways by HRP. (A) HPLC results of the phenol degradation products at different reaction times: (1) phenol standard, (2) 10 min, (3) 20 min, (4) 50 min, and (5) 2 h. (B) Color changes of phenol degradation at different times and (C) mechanisms and pathways for the enzymatic degradation of phenol by HRP.

MCM-41(H) displays the smallest k_d value, indicating that it has the highest thermal stability. The half-life ($t_{1/2}$) and D-value of the enzyme gradually decrease with increasing temperature. The data in Tables S2−S4 show that the $t_{1/2}$ of the enzyme at 60 °C is extended from 202.51 min (free enzyme) to 484.75 min [HRP@Al-MCM-41(H)] after immobilization. Moreover, the $t_{1/2}$ and D-value of the immobilized samples are extended, indicating that the immobilization treatment improves the thermal stability of the enzyme. The activation energy required for thermal deactivation (E_d) is higher for the immobilized enzyme than the free enzyme,[42] indicating that the stability of the immobilized enzyme is higher than that of the free enzyme (Table S5). High temperatures destroy the spatial structure of enzymes,[43] and the thermal deactivation of enzyme proteins is accompanied by the breakage of weak intermolecular interactions (e.g., hydrophobic interactions, hydrogen bonds, van der Waals interactions, and ionic bonds).[44] However, covalent bonds are formed between the carrier and HRP that stabilize the three-dimensional structure of the immobilized enzyme during heat treatment; therefore, it retains its catalytic activity.

3.5. Enzyme Stability. The free and immobilized enzymes were stored at a temperature of 4 or 25 °C for 30 d, during which the enzyme activity was measured every 5 d. The residual enzyme activities at the two temperatures were calculated, and the storage stability results are shown in Figure 6. The residual activities of the free and immobilized enzymes gradually decrease with time. All three enzyme samples retain 90% of their activity at 4 °C (Figure 6A). In contrast, the residual activity of the free enzyme decreases to 20% after 30 d at 25 °C, while those of the immobilized enzymes only decrease to ~60% under the same conditions (Figure 6B,C).

These results, therefore, reveal that the enzyme can be preserved for longer times after immobilization. We tested the reusability of the immobilized enzyme by conducting cyclic degradation−separation experiments. The enzyme activity decreases significantly after each cycle (Figure S4), which may be because HRP detaches from the Al-MCM-41 carrier during use, which reduces the activity of the immobilized enzyme in subsequent cycles. It is also possible that light caused the enzyme activity to decrease during repeated use; the porphyrin ring in HRP, which acts as the ligand of the enzyme and plays a crucial role in its structure and activity, is light-sensitive.[45] Specifically, light destroys the molecular structure of the porphyrin ring, leading to enzyme deactivation under light exposure.

3.6. Enzymatic Degradation of Phenol. We used immobilized HRP to degrade phenol. The enzyme was mixed with phenol for the degradation reaction, and the phenol contents in the reaction solution at different reaction times were determined by liquid chromatography; the results are presented in Figure 7A. The retention time of phenol in the liquid chromatogram is 6.5 min, and the detection value of phenol in the sample gradually decreases with increasing reaction time. Notably, the degradation rate of phenol exceeds 80% within 10 min.

Interesting color changes are also observed during the degradation of phenol (Figure 7B): at 0−1 h, the color of the reaction solution gradually changes from colorless to coffee brown and continues to become darker as the degradation of phenol by the enzyme proceeds. After 1 h, the color of the reaction solution gradually becomes lighter with increasing reaction time, and at 24 h, it becomes colorless.

The process of substance transformation in the reaction solution was studied using mass spectrometry. The proposed

mechanism of the conversion process (Figure 7C) is as follows: H_2O_2 is catalyzed by HRP to produce $^\bullet OH$ and $^\bullet O_2^-$ radicals. Phenol is then catalyzed by the $^\bullet O_2^-$ radicals to produce hydroquinone, which is in turn oxidized to produce *p*-benzoquinone. The interaction of *p*-benzoquinone and hydroquinone in solution produces quinhydrone, resulting in a color change from colorless to brown. In the presence of $^\bullet OH$ and $^\bullet O_2^-$ radicals, *p*-benzoquinone and *p*-benzenediol form 2,2′-dihydroxybiphenyl. The dihydroxybiphenyl is oxidized by ring opening to form small molecules of acid,[46] and the solution turns colorless. The above results indicate that phenol undergoes a complex transformation process under the action of enzymatic degradation.

4. CONCLUSIONS

The enzymatic degradation of phenol is an environmentally friendly process; however, HRP is easily inactivated by environmental conditions such as temperature and pH. Thus, it is difficult to apply this strategy to large-scale phenol degradation. Improving the stability of HRP is therefore a prerequisite for large-scale application. With this in mind, in this study, we improved the enzyme performance by immobilization modifications. Notably, after immobilization, the half-life of the enzyme was increased from 745.17 min (free enzyme) to 1968.02 min (HRP@Al-MCM-41(H)) at 50 °C and from 202.51 min to 484.75 min, respectively, at 60 °C. Moreover, we applied the HRP@Al-MCM-41(H) to degrade phenol, wherein 80% phenol conversion was attained within 10 min, and the intermediate metabolites of phenol were completely degraded within 24 h. Finally, the process and mechanism of phenol degradation were elucidated to clarify the process of phenol degradation by HRP. This is an important reference for the enzymatic degradation of phenol. Our developed method provides a promising technical solution for the degradation of phenol in aqueous environments using immobilized enzymes.

ASSOCIATED CONTENT

Supporting Information
The Supporting Information is available free of charge at https://pubs.acs.org/doi/10.1021/acsomega.3c01570.

Kinetic parameters for the thermal deactivation study and activation energy for the enzyme thermal deactivation (E_d) of the free and immobilized enzymes; LC–MS ion fragmentation; flow chart of the preparation of the immobilized enzymes; XRD patterns of the immobilized enzymes; and reusability of the immobilized enzymes (PDF)

AUTHOR INFORMATION

Corresponding Author
Lanqing Ma − *Key Laboratory for Northern Urban Agriculture of Ministry of Agriculture and Rural Affairs and Beijing Advanced Innovation Center for Tree Breeding by Molecular Design, Beijing University of Agriculture, Beijing 102206, PR China;* orcid.org/0000-0002-5578-6958; Phone: +86-10-80797305; Email: lqma@bua.edu.cn; Fax: +86-10-80797305

Authors
Can Liu − *Key Laboratory for Northern Urban Agriculture of Ministry of Agriculture and Rural Affairs, Beijing University*

of Agriculture, Beijing 102206, PR China; orcid.org/0000-0002-2036-0826

Li Tan − *Key Laboratory for Northern Urban Agriculture of Ministry of Agriculture and Rural Affairs, Beijing University of Agriculture, Beijing 102206, PR China*

Kaixin Zhang − *Key Laboratory for Northern Urban Agriculture of Ministry of Agriculture and Rural Affairs, Beijing University of Agriculture, Beijing 102206, PR China*

Wenyi Wang − *Key Laboratory for Northern Urban Agriculture of Ministry of Agriculture and Rural Affairs, Beijing University of Agriculture, Beijing 102206, PR China*

Complete contact information is available at:
https://pubs.acs.org/10.1021/acsomega.3c01570

Author Contributions
C.L. and L.T. contributed equally to this work. Lanqing Ma and Can Liu designed the experiments. Li Tan and Wenyi Wang performed the experiments. Can Liu and Kaixin Zhang analyzed the data. Can Liu and Li Tan wrote the manuscript. All authors contributed to the article and approved the submitted version.

Notes
The authors declare no competing financial interest.

REFERENCES
(1) Ray, S.; Senapati, T.; Sahu, S.; Bandyopadhyaya, R.; Anand, R. Design of Ultrasensitive Protein Biosensor Strips for Selective Detection of Aromatic Contaminants in Environmental Wastewater. *Anal. Chem.* **2018**, *90*, 8960−8968.
(2) Zhang, J.; Zhang, N.; Tack, F.; Sato, S.; Alessi, D. S.; Oleszczuk, P.; Wang, H.; Wang, X.; Wang, S. Modification of ordered mesoporous carbon for removal of environmental contaminants from aqueous phase: A review. *J. Hazard. Mater.* **2021**, *418*, 126266.
(3) Buckley, J. D.; Meadows, A. T.; Kadin, M. E.; Le Beau, M. M.; Siegel, S.; Robison, L. L. Pesticide exposures in children with non-Hodgkin lymphoma. *Cancer* **2000**, *89*, 2315−2321.
(4) Li, X. Y.; Cui, Y. H.; Feng, Y. J.; Xie, Z. M.; Gu, J. D. Reaction pathways and mechanisms of the electrochemical degradation of phenol on different electrodes. *Water Res.* **2005**, *39*, 1972−1981.
(5) Rehman, G. U.; Tahir, M.; Goh, P. S.; Ismail, A. F.; Hafeez, A.; Khan, I. U. Enhancing the photodegradation of phenol using Fe3O4/SiO2 binary nanocomposite mediated by silane agent. *J. Phys. Chem. Solids* **2021**, *153*, 110022.
(6) Wood, R. J.; Bertin, A.; Lee, J.; Bussemaker, M. J. The application of flow to an ultrasonic horn system: Phenol degradation and sonoluminescence. *Ultrason. Sonochem.* **2021**, *71*, 105373.
(7) Yang, G.; Chen, H.; Qin, H.; Feng, Y. Amination of activated carbon for enhancing phenol adsorption: Effect of nitrogen-containing functional groups. *Appl. Surf. Sci.* **2014**, *293*, 299−305.
(8) Tran, T. V.; Cao, V. D.; Nguyen, V. H.; Hoang, B. N.; Vo, D. V. N.; Nguyen, T. D.; Bach, L. G. MIL-53 (Fe) derived magnetic porous carbon as a robust adsorbent for the removal of phenolic compounds under the optimized conditions. *J. Environ. Chem. Eng.* **2020**, *8*, 102902.
(9) Villegas, L. G. C.; Mashhadi, N.; Chen, M.; Mukherjee, D.; Taylor, K. E.; Biswas, N. A Short Review of Techniques for Phenol Removal from Wastewater. *Curr. Pollut. Rep.* **2016**, *2*, 157−167.
(10) Pacheco, M.; Morão, A.; Lopes, A.; Ciríaco, L.; Gonçalves, I. Degradation of phenols using boron-doped diamond electrodes: A

method for quantifying the extent of combustion. *Electrochim. Acta* **2007**, *53*, 629−636.

(11) Eżerskis, Z.; Jusys, Z. Electropolymerization of chlorinated phenols on a Pt electrode in alkaline solution Part I: A cyclic voltammetry study. *J. Appl. Electrochem.* **2001**, *31*, 1117−1124.

(12) Bagal, M. V.; Gogate, P. R. Wastewater treatment using hybrid treatment schemes based on cavitation and Fenton chemistry: A review. *Ultrason. Sonochem.* **2014**, *21*, 1−14.

(13) Neyens, E.; Baeyens, J. A review of classic Fenton's peroxidation as an advanced oxidation technique. *J. Hazard. Mater.* **2003**, *98*, 33−50.

(14) Bello, M. M.; Abdul Raman, A. A.; Asghar, A. A review on approaches for addressing the limitations of Fenton oxidation for recalcitrant wastewater treatment. *Process Saf. Environ.* **2019**, *126*, 119−140.

(15) Chowdhuryi, A. H.; et al. Plasmid Mediated Degradation of Phenol by Two Bacterial Strains Pseudomonas sp. and Staphylococcus sp. *Pak. J. Biol. Sci.* **2000**, *3*, 939−942.

(16) Banerjee, A.; Ghoshal, A. K. Phenol degradation by Bacillus cereus: Pathway and kinetic modeling. *Bioresour. Technol.* **2010**, *101*, 5501−5507.

(17) Pazarlioglu, N. K.; Telefoncu, A. Biodegradation of phenol by Pseudomonas putida immobilized on activated pumice particles. *Process Biochem.* **2005**, *40*, 1807−1814.

(18) Prieto, M.; Hidalgo, A.; Rodríguez-Fernández, C.; Serra, J.; Llama, M. Biodegradation of phenol in synthetic and industrial wastewater by Rhodococcus erythropolis UPV-1 immobilized in an air-stirred reactor with clarifier. *Appl. Microbiol. Biotechnol.* **2002**, *58*, 853−859.

(19) Jemaat, Z.; Suárez-Ojeda, M.; Pérez, J.; Carrera, J.; Carrera, Z. J.; Julio, P. Sequentially alternating pollutant scenarios of phenolic compounds in a continuous aerobic granular sludge reactor performing simultaneous partial nitritation and o-cresol biodegradation. *Bioresour. Technol.* **2014**, *161*, 354−361.

(20) Liu, Z. F.; Zeng, G. M.; Zhong, H.; Yuan, X. Z.; Fu, H. Y.; Zhou, M. F.; Ma, X. L.; Li, H.; Li, J. B. Effect of dirhamnolipid on the removal of phenol catalyzed by laccase in aqueous solution. *World J. Microbiol. Biotechnol.* **2012**, *28*, 175−181.

(21) Jiang, W.; Yang, J.; Wang, X.; Han, H.; Yang, Y.; Tang, J.; Li, Q. Phenol degradation catalyzed by a peroxidase mimic constructed through the grafting of heme onto metal-organic frameworks. *Bioresour. Technol.* **2018**, *247*, 1246−1248.

(22) Seetharam, G. B.; Saville, B. A. Degradation of phenol using tyrosinase immobilized on siliceous supports. *Water Res.* **2003**, *37*, 436−440.

(23) Hinteregger, C.; Leitner, R.; Loidl, M.; Ferschl, A.; Streichsbier, F. Degradation of phenol and phenolic compounds by Pseudomonas putida EKII. *Appl. Microbiol. Biotechnol.* **1992**, *37*, 252−259.

(24) Sheldon, R. A.; van Pelt, S. Enzyme immobilisation in biocatalysis: why, what and how. *Chem. Soc. Rev.* **2013**, *42*, 6223−6235.

(25) Zhang, F. Study on the removal of phenolic wastewater catalyzed by horseradish peroxidase. *Appl. Chem. Ind.* **2012**, *41*, 1204−1207.

(26) Zhou, Z.; Hartmann, M. Progress in enzyme immobilization in ordered mesoporous materials and related applications. *Chem. Soc. Rev.* **2013**, *42*, 3894−3912.

(27) Chen, X.; Huang, L.; Ding, G.; Li, Q. Characterization and catalytic performance of mesoporous molecular sieves Al-MCM-41 materials. *Catal. Lett.* **1997**, *44*, 123−128.

(28) Yu, D.; Zhang, X.; Wang, T.; Geng, H.; Wang, L.; Jiang, L.; Elfalleh, W. Immobilized Candida antarctica lipase B (CALB) on functionalized MCM-41: Stability and catalysis of transesterification of soybean oil and phytosterol. *Food Biosci.* **2021**, *40*, 100906.

(29) Xc, A.; Jl, A.; Ya, H.; Xin, Z.; Shuang, Y.; Yw, B.; Wei, L.; Zg, B.; Yl, A.; Fa, X. Insight into the Effect of Lewis Acid of W/Al-MCM-41 Catalyst on Metathesis of 1-Butene and Ethylene. *Appl. Catal., A* **2020**, *604*, 117772.

(30) Zermeo, B. B.; García-Alamilla, M. E. R. Photocatalytic degradation of phenol and 4-chlorophenol with titania, oxygen and ozone. *Sustainable Environ. Res.* **2011**, *21*, 299−305.

(31) Kozyrev, S. V.; Volovich, I. V. The Arrhenius formula in kinetic theory and Witten's spectral asymptotics. *J. Phys. A: Math. Theor.* **2011**, *44*, 215202.

(32) Vishwasrao, C.; Ananthanarayan, L. Kinetics of inactivation of quality-deteriorating enzymes and degradation of selective phytoconstituents in pink guava pulp during thermal processing. *J. Phys. A: Math. Theor.* **2018**, *55*, 3273−3280.

(33) Sanjay, G.; Sugunan, S. Enhanced pH and thermal stabilities of invertase immobilized on montmorillonite K-10. *Food Chem.* **2006**, *94*, 573−579.

(34) El-Naggar, M. E.; Abdel-Aty, A. M.; Wassel, A. R.; Elaraby, N. M.; Mohamed, S. A.; Wassel; Nesma, M.; Elaraby; Saleh, A.; Mohamed. Immobilization of horseradish peroxidase on cationic microporous starch: Physico-bio-chemical characterization and removal of phenolic compounds. *Int. J. Biol. Macromol.* **2021**, *181*, 734−742.

(35) Jankowska, K.; Zdarta, J.; Grzywaczyk, A.; Degórska, O.; Kijeńska-Gawrońska, E.; Pinelo, M.; Jesionowski, T. Horseradish peroxidase immobilised onto electrospun fibres and its application in decolourisation of dyes from model sea water. *Process Biochem.* **2021**, *102*, 10−21.

(36) Lopes, L. C.; Barreto, M. T. M.; Gonçalves, K. M.; Alvarez, H. M.; Heredia, M. F.; de Souza, R. O. M. A.; Cordeiro, Y.; Dariva, C.; Fricks, A. T. Stability and structural changes of horseradish peroxidase: Microwave versus conventional heating treatment. *Enzyme Microb. Technol.* **2015**, *69*, 10−18.

(37) Abdel-Naby, M. A.; Ahmed, S. A.; Wehaidy, H. R.; El-Mahdy, S. A. Catalytic, kinetic and thermodynamic properties of stabilized Bacillus stearothermophilus alkaline protease. *Int. J. Biol. Macromol.* **2017**, *96*, 265−271.

(38) Moussa, S.; Chhin, D.; Pollegioni, L.; Mauzeroll, J. Quantitative measurements of free and immobilized RgDAAO Michaelis-Menten constant using an electrochemical assay reveal the impact of covalent cross-linking on substrate specificity. *Anal. Bioanal. Chem.* **2021**, *413*, 6793−6802.

(39) Melo, M. N.; Pereira, F. M.; Rocha, M. A.; Ribeiro, J. G.; Diz, F. M.; Monteiro, W. F.; Ligabue, R. A.; Severino, P.; Fricks, A. T. Immobilization and characterization of Horseradish Peroxidase into Chitosan and Chitosan/PEG nanoparticles: A comparative study. *Process Biochem.* **2020**, *98*, 160−171.

(40) Liu, X.; Zhang, Q.; Li, M.; Qin, S.; Zhao, Z.; Lin, B.; Ding, Y.; Xiang, Y.; Li, C. Horseradish peroxidase (HRP) and glucose oxidase (GOX) based dual-enzyme system: Sustainable release of H2O2 and its effect on the desirable ping pong bibi degradation mechanism. *Environ. Res.* **2023**, *229*, 115979.

(41) Fu, D.; Li, C.; Lu, J.; Rahman, A. U.; Tan, T. Relationship between thermal inactivation and conformational change of Yarrowia lipolytica lipase and the effect of additives on enzyme stability. *J. Mol. Catal. B: Enzym.* **2010**, *66*, 136−141.

(42) Bravo Rodríguez, V.; et al. Thermal deactivation of a commercial α-amylase from Bacillus licheniformis used in detergents. *Biochem. Eng. J.* **2006**, *27*, 299−304.

(43) Fink, A. L.; Behner, K. M.; Tan, A. K. Kinetic and structural characterization of reversibly inactivated .beta.-lactamase. *Biochemistry* **1987**, *26*, 4248−4258.

(44) Chang, D. K.; Cheng, S. F.; Yang, S. H. A helix initiation motif, XLLRA, is stabilized by hydrogen bond, hydrophobic and van der Waals interactions. *Biochim. Biophys. Acta, Protein Struct. Mol. Enzymol.* **2000**, *1478*, 39−50.

(45) Tang, Q.; Gong, T.; Cao, H.; Wang, L.; Li, R.; Zheng, X. Study on the changes and mechanisms of photocatalytic activity of horseradish peroxidase induced by light. *Spectrosc. Spect. Anal.* **2018**, *38*, 3692−3698.

(46) Othman, I.; Hisham Zain, J.; Abu Haija, M.; Banat, F. Catalytic activation of peroxymonosulfate using CeVO$_4$ for phenol degradation:

An insight into the reaction pathway. *Appl. Catal., B* **2020**, *266*, 118601.